

1 **The role of matric potential, solid interfacial chemistry and wettability on isotopic**
2 **equilibrium fractionation.**

3

4 **Authors:** Marcel Gaj^{1,2}, Axel Lamparter², Susanne K. Woche³, Jörg Bachmann³, Jeffrey J.
5 McDonnell^{1,4,5}, C. Florian Stange²

6

7 **Author affiliations:**

8 ¹ Global Institute for Water Security, School of Environment and Sustainability, University
9 of Saskatchewan, Saskatoon, Canada

10 ²Federal Institute for Geosciences and Natural Resources, Soil as a Resource-Properties
11 and Dynamics, Hannover, Germany

12 ³ Leibniz University, Institute of Soil Science, Hannover, Germany

13 ⁴School of Geography, Earth & Environmental Sciences, University of Birmingham,
14 Birmingham, UK

15 ⁵School of Environmental Science and Engineering, South University of Science and
16 Technology of China, Shenzhen, China

17

18

19 **Corresponding author:**

20 Marcel Gaj

21 marcel.gaj@bgr.de

22

23 **Submit to: Vadose Zone Journal**

24

25

26

27

28

29 **Core ideas:**

30 - Matric potential controls the equilibrium fractionation factor between soil water
31 stable isotopes and water vapor

32 - Surface chemistry as determined by X-ray photoelectron spectroscopy affects the
33 equilibrium fractionation factor

34 - A conceptual isotope retention characteristic approach is presented

35

36

37

38

39

40

41

42

43

44

45

46 **Keywords:** water stable isotopes, isotope retention curve, matric potential, water
47 repellency, evaporation

48

49

50

51

52

53 Abstract

54 Soil water stable isotopes are widely used for geo- and eco-hydrological applications.
55 However, the signature of soil water isotopic composition in the environment depends on
56 various factors. While recent work has shown matric potential effects on equilibrium
57 fractionation, little work has examined other soil parameters concerning soil water energy
58 status like the surface wettability, usually quantified in terms of contact angle.

59 Here we explore simultaneously the role of matric potential, contact angle and soil surface
60 chemistry effects on the equilibrium fractionation factor during soil water evaporation. We
61 present a simple laboratory experiment with four different soils of various textures.
62 Subsamples of each texture class were treated with dichlorodimethylsilane to modify
63 surface wetting properties. Additionally, we tested two natural soil samples to explore
64 wettability effects. Samples were dried at temperatures between 40°C and 550°C to
65 produce chemically modified surface properties. All samples were spiked with water of
66 known isotopic composition at different water contents. The isotopic signature was
67 determined using the vapor-bag equilibration method. Matric potential of each sample was
68 measured with a soil water potential meter, the contact angle was determined with the
69 sessile drop method and the surface chemistry by X-ray photoelectron spectroscopy.

70 In addition to temperature and soil matric potential, the elemental composition has
71 apparently some control on the equilibrium fractionation factor. Based on findings, we
72 introduce a new soil water isotope retention characteristic approach to summarize how all
73 these factors (matric potential, contact angle and soil surface chemistry) each control the
74 equilibrium fractionation factor for $^{18}\text{O}/^{16}\text{O}$ and $^2\text{H}/\text{H}$. Corresponding retention curve
75 approach parameters are promising to be applied in the future to predict soil water
76 fractionation effects under natural and non-stationary conditions.

77

78

79 **Introduction**

80 The storage and mixing of water in the unsaturated zone is dominated by various
81 processes that interact with physical, chemical and biological properties of the soil
82 (Vereecken et al., 2016; Pronk et al., 2017). In this context, stable isotopes are a powerful
83 tool to investigate water and water vapor exchange processes between soil and
84 atmosphere (Dawson et al, 2002). For instance to trace hydrological processes of
85 terrestrial ecosystems, including subsurface flow path ways (Garvelmann et al., 2012;
86 Stumpp and Maloszewski (2010); Mueller et al., 2014, Oshun et al., 2016), travel times
87 (Klaus et al., 2015; Sprenger et al., 2016), groundwater recharge (Koeniger et al, 2016),
88 evapotranspiration (Dubbert et al., 2013; Gaj et al., 2016), plant root water uptake (Vargas
89 et al., 2017, Rothfuss and Javaux, 2017) and the partitioning of the global terrestrial water
90 cycle (Evaristo et al, 2015; Good et a., 2015; Bowen, 2015; McDonnell, 2014).

91

92 *Stable isotope fractionation theory*

93 The isotopic signature of precipitation is depleted in ^{18}O and ^2H under cold environmental
94 conditions and enriched under warm environmental conditions. This results in seasonal
95 differences and is reflected in the slope of the global meteoric water line (GMWL),
96 considering the earth to be a closed system (Craig and Gordon, 1965; Clark and Fritz,
97 1997). The different vapor pressures of H_2^{18}O and $^2\text{H}^1\text{H}^{16}\text{O}$ in equilibrium with the water
98 vapor pressure result in an enrichment of ^2H in the water phase which is eight times
99 greater than correspondingly for the ^{18}O isotope. In addition to equilibrium fractionation,
100 evaporation entails further kinetic fractionation effects depending on surface temperature,
101 wind speed and relative humidity. At low or zero relative humidity (RH $\sim 0\%$), the isotopic
102 enrichment follows a Rayleigh distillation, which means that the isotopic signature of the
103 evaporating water can be simply described by the Rayleigh-equation. However, under
104 atmospheric conditions, humidity will mostly be $> 0\%$. Then additional fractionation is

105 caused by kinetic effects due to the different diffusivities of H_2^{16}O , DH^{16}O and H_2^{18}O (Clark
106 and Fritz, 1997, Horita et al., 2008) in the liquid and gas phase. During the evaporation
107 process, water vapor diffuses through a transition zone from a boundary layer above the
108 water surface into the atmosphere and vice versa. This is codified in the well-known Craig
109 and Gordon model (Craig and Gordon, 1965). The combined equilibrium and kinetic
110 fractionation effects result in local evaporation lines (LEL) of water from open water bodies
111 with slopes lower than the GMWL (Gat, 2000). The slopes of evaporation lines of open
112 water bodies are related to different environmental conditions like the relative humidity and
113 can be determined using stable isotope signatures of the water (Gonfiantini, 1986;
114 Skrypek et al., 2015). Tracing soil water infiltration and groundwater recharge can be
115 done by simply tracking the time series of precipitation isotope signature and mixing,
116 lagging and damping can be used to estimate travel times through the soil profile (McGuire
117 and McDonnell, 2006). Also labeling experiments can be used to track soil water
118 movement and water uptake as summarized in recent reviews (Koeniger et al., 2016;
119 Sprenger et al., 2016)

120

121 *Theory for isotope fractionation for subsurface water*

122 Compared to the theory applied for stable isotope surface hydrology, the theory for isotope
123 fractionation for subsurface water is more complex. Evaporation from the soil profile as
124 traced by stable isotopes is affected additionally by soil physical properties. Early
125 benchmark presented theoretical and analytical approaches (Barnes and Allison, 1983) to
126 calculate steady state in isothermal and non-steady state/ non-isothermal soil profiles
127 (Barnes and Allison, 1984). These authors further showed experimentally that the slope of
128 the LEL is controlled by the diffusivity of the water vapor, the tortuosity of the soil pore
129 system and the evaporation rate (Allison and Barnes, 1988). These experiments were re-
130 examined with subsequent numerical studies (Braud et al., 2009a, Braud et al., 2009b,

131 Rothfuss et al., 2012) and later with higher temporal resolution using in-situ approaches
132 (Rothfuss et al., 2015). Model results suggested that the kinetic fractionation factor is
133 associated with the highest uncertainty especially at the dry end of the water retention
134 curve at low relative humidity. For wet soil, the relative humidity in the pore space is a
135 function of temperature and the energy status of pore water. Decreasing soil moisture
136 increases the matric potential, i.e. the pressure difference to atmospheric pressure, and
137 reduces the relative humidity in the pore space (Figure 1).

138 **Figure 1**

139 As a consequence, methods to determine the isotopic signature from immobile soil water
140 in comparison to bulk water can be difficult and can bias the isotopic signature of soil water
141 depending on the soil water content (Wassenaar et al., 2008; Hendry et al., 2015), the
142 texture (Orlowski et al., 2016; Königer et al., 2011; West et al., 2006), i.e. effects of
143 hydrated cations in the interlayer space of clay minerals (Oerter et al., 2014, Gaj et al.,
144 2017a; Gaj et al., 2017b) and the presence of soil carbonate (Meißner et al., 2013).
145 Available methods to determine soil water isotopic signatures were reviewed and
146 theoretically discussed (Sprenger et al., 2015). In an extensive laboratory study some of
147 these methods were compared using spiked water isotope experiments (Orlowski et al.,
148 2016). It was found that methods that do not require a phase change (i.e. squeezing and
149 centrifugation) did best in recovering the isotopic signature of the spiked water. However,
150 the direct vapor equilibration method (Wassenaar et al., 2008, Hendry et al., 2015) has
151 strong potential for future application because portable laserspectrometers allow vapor
152 sampling in-situ (Rothfuss et al., 2013; Volkmann and Weiler, 2014, Gaj et al., 2016,
153 Oerter and Bowen, 2017). This will increase the spatial and temporal resolution of isotope
154 data reflecting the heterogeneity of water and water vapor fluxes. The time required to
155 reach isotopic equilibrium between soil water and water vapor can vary from minutes in
156 sandy soil as shown in a field application (Gaj et al., 2016) and for a column experiment in

157 the laboratory (Rothfuss et al., 2015). Depending on the texture of the soil sample
158 equilibrium can also take a few hours to several days after destructive sampling, using the
159 vapor bag equilibration method (Wassenaar et al., 2008; Garvelman et al., 2012; Hendry
160 et al., 2015; Sprenger et al., 2015). Direct equilibration methods assume the equilibrium
161 fractionation factor is a function of temperature as it is for open water surfaces (Majoube et
162 al., 1970; Wassenaar et al., 2008). Also, other stable isotope related model assumptions
163 such as Rayleigh distillation (Clark and Fritz, 1997), the Craig and Gordon model (Craig
164 and Gordon, 1965) or the non-steady-state leaf water isotope model (Dongmann et al.,
165 1974) require the equilibrium fractionation factor for their application. It has been
166 discussed that relative humidity might control the kinetic fractionation factor (Soderberg et
167 al., 2012). Adsorption experiments showed that the equilibrium fractionation factor is
168 controlled by the vapor pressure (Lin and Horita, 2016; Lin et al., 2017). Other recent work
169 has been shown that the equilibrium fractionation factor of natural soil samples is
170 controlled by matric potential, which, in turn, control the water vapor pressure.

171

172 So, what is the way forward? We know that the physical properties of soils are linked to
173 the pore size distribution, which is affected by soil texture, soil bulk density as well as the
174 organic matter content (Figure 1). Water retention characteristics are parameterized in
175 well-known water retention models and their derivatives (Brooks and Corey, 1964; van
176 Genuchten, 1980; Othmer et al., 1991; Peters et al., 2015). In some soils, water retention
177 characteristics are further altered significantly by specific interfacial properties of the
178 particles, because the formation of biogeochemical interfaces (BGI's) may develop in
179 some soils water repellent surfaces on the pore surfaces (Bachmann and van der Ploeg,
180 2002). These changes in wettability also change the shape of the water retention curve to
181 virtually coarser texture (Bisdorf et al., 1993; Bauters et al., 2000; Reszkowska et al., 2014;
182 Liu et al., 2011). Wettability properties can also change over time depending on moisture

183 conditions and the composition of the biogeochemical interface (de Jonge et al., 2007). As
184 illustrated in Figure 2 (left), capillary pressure of the liquid phase, which is basically the
185 pressure difference above a curved water meniscus and the pressure inside the meniscus,
186 is also related to the contact angle (CA) that forms at the three-phase boundary of the
187 unsaturated solid-liquid-gas system (Bachmann et al., 2007; Bauters et al., 2000). In this
188 respect, the type of adsorbed cation has been found to be insignificant for wetting
189 properties (Diehl et al., 2014). However, the abundance of cations and their effect on soil
190 organic matter interfacial properties is physically and chemically not yet fully understood
191 (Pronk et al., 2017). Recently it was found for numerous soils that there is a significant
192 relationship between the wettability (expressed in the CA) and the surface C/O ratio
193 (Woche et al., 2017). However, the link between the wettability in a solid-liquid-gas system
194 and its effect on isotopic fractionation has not yet been examined. Therefore, the objective
195 of the present study is: What is the relative role of matric potential, wettability and soil
196 surface chemistry on the soil water isotopic equilibrium fractionation factor?

197 **Figure 2**

198

199 **Methods**

200 In order to answer these questions, we analyzed soil samples of different textures and
201 samples with similar textures, but with different surface properties to cover i.e.: i) wide
202 range of textures, but not swelling/shrinking, ii) differences in wettability (moderate T-
203 treatment), iii) differences in interfacial chemistry (salinization, 550° treatment), iv) model
204 soils vs. natural soils to increase complexity of interface

205

206 *Sample description*

207 The schematic of the sample preparation procedure is illustrated and explained in Figure 2
208 (right). Soil samples with different texture (refer to Table 1) were artificially hydrophobized

209 by treatment with dichlorodimethylsilane (DCDMS) (Goebel et al., 2013; Hassan et al.,
210 2014). An additional set of samples was collected from an agricultural field and a nearby
211 (approx. 20m) located coniferous forest (*Pinus sylvestris L.*). The two samples with the
212 same texture but different wettability properties were split into 3 sub samples. The sub
213 samples were temperature treated (dried for 24h at 40, 105, and 550°C) to create different
214 surface properties. All samples were subsequently analyzed for texture, surface elemental
215 composition, contact angle and specific surface area / BET.

216

217 *Isotope measurements*

218 The well-known direct equilibration approach was used to determine stable isotope
219 signatures of the soil water (Wassenaar et al, 2008). This method assumes that soil
220 water quickly reaches thermodynamic equilibrium with the vapor in the head space. Then
221 the bag head space (i.e. the vapor) was measured with a water vapor isotope analyzer
222 (WVIA, LGR, IWA-35-EP). Isotope signatures are reported in δ -notation. The δ refers to
223 the measured isotope ratios of the sample R_{sample} to an international or laboratory
224 reference standard $R_{\text{reference}}$:

225

$$226 \quad \delta = \left(\frac{R_{\text{sample}}}{R_{\text{reference}}} - 1 \right) \quad [1]$$

227

228 The isotope ratio R is defined as the quotient of $N(^iE)_P$ and $N(^jE)_P$, with the number of
229 each isotope iE and jE , of chemical element E in substance P expressed as (Coplen,
230 2011):

231

$$232 \quad R(^iE/^jE) = \frac{N(^iE)_P}{N(^jE)_P} \quad [2]$$

233

234 The laboratory standards had δ -values of 200.4 ‰ and -26.2 ‰ for the enriched and
235 3.0 ‰ and -0.1 ‰ for the depleted standard for ^2H and ^{18}O , respectively. All samples were
236 normalized with a two-point calibration using the laboratory standards. The laboratory
237 standards were calibrated to the international reference scale VSMOW-SLAP.

238 We calculated our tension-based fractionation factor $\alpha^{i/j}E_{P/Q}$ based on the isotope ratio of
239 the labelled water $R(^i\text{E}/^j\text{E})_Q$ and the isotope ratio of the measured water vapor $R(^i\text{E}/^j\text{E})_P$
240 as follows:

241

$$242 \quad \alpha^{i/j}E_{P/Q} = \frac{R(^i\text{E}/^j\text{E})_P}{R(^i\text{E}/^j\text{E})_Q} = \frac{1000+\delta_P}{1000+\delta_Q} = a_{x-y} \quad [3]$$

243

244 where a_{x-y} is used as simplified notation for the equilibrium fractionation factor.

245

246 *Sample Preparation and measurement procedure*

247 All DCDMS-treated soil samples and their non-treated controls (each 100g) were oven
248 dried at 105°C for 24h and subsequently labeled with deionized water of known isotopic
249 signature. Soil water contents in the range from 0.1% to 6% of the weight of the soil
250 sample were prepared in individual zip-loc bags.

251 In order to preserve the surface properties achieved by drying at specific temperatures, the
252 two soil samples had been spiked after thermal treatment for 24h at 40°C and 105°C. The
253 samples treated with 550°C were also again dried at 105°C prior to the spiking. All
254 samples were cooled down to room temperature after placing them into an exicator. In
255 contrast to the DCDMS-treated sample set, the headspace measurements were done 1h,
256 24h and 72h after adding the spiked water to the 200g soil sample. After each headspace
257 measurement a subsample was measured for soil tension with the WP4 water potential
258 meter as explained below. Bags were immediately sealed after subsamples were taken
259 out. The headspace was not refilled with dry air to avoid evaporation effects. Instead,

260 vapor of the headspace was circulated through the laserspectrometer. After emerging a
261 needle into the zip-loc bag headspace gas from the bags has been extracted into the
262 instrument. When the measured mixing ratio approached its maximum a second needle
263 was emerged in to the bags. This second needle returned the exhaust flow of the analyser
264 into the bags. On that way the gas was circulated between the analyser and the bag. The
265 bags and the transport lines have the same temperature. Hence there is no condensation
266 during the sampling procedure (isothermal conditions). All standards were measured in the
267 same way. A quality check standard was measured with each sequence. A quality check
268 standard is water of known isotopic composition treated as the samples. After
269 normalization of the data the known value of the quality check is compared to the
270 measured value. The difference between the two are the numbers that we provide with
271 0.4‰ for $\delta^{18}\text{O}$ -values and 2.32 ‰ for $\delta^2\text{H}$ -values. This is per definition the trueness of your
272 measurement procedure (Barwick and Prichard, 2011).

273 To account for the water loss by evaporation into the headspace of the sample bags, the
274 theoretical new equilibrium fractionation factor was calculated according to Gat (1994)
275 with:

276

$$277 \quad R_f = \frac{R_0}{\alpha - f(\alpha - 1)} \quad [4]$$

278

279 where R_0 is the initial isotope ratio, R_f the isotope ratio of the remaining fraction f .
280 According to equation 4 the mean enrichment due to a water loss into the headspace was
281 0.14‰ for $\delta^{18}\text{O}$ -values and 1.15 ‰ for $\delta^2\text{H}$ -values. Water amount effects are therefore
282 camouflaged by the accuracy of our bag method as determined from the quality check.
283 Further, mixing ratio dependencies of the laserspectrometer were considered and were
284 insignificant within the range we measured.

285

286 *Soil tension measurements*

287 Matric potential was measured on a WP4C water potential meter (Decagon Devices, Inc.,
288 Pullman, WA). This psychrometer device has a precision of ± 0.1 Mpa between 0 to -10 Mpa
289 and $\pm 1\%$ between -10 to -300 Mpa (Gubiani et al., 2013). The water potential meter
290 measures the combined osmotic (ψ_{os}) and matric potential (ψ_m). The osmotic potential was
291 determined from the electrical conductivity (EC) of the soil solution after adding 50 ml of
292 deionized water to 100g of soil sample. Then ψ_{os} can be calculated as recommended in
293 the manual of the WP4:

294

$$295 \psi_{os} = -0.036EC \left(\frac{\theta_s}{\theta} \right) \quad [5]$$

296

297 with EC [dS m^{-1}] denotes for electrical conductivity of the solution, θ_s [g/g] for the water
298 content at saturation and θ [g/g] for the actual water content. Then water retention curves
299 were plotted from the known gravimetric water content and the calculated matric potential
300 (combined potential minus osmotic potential).

301

302 *X-ray photoelectron spectroscopy (XPS)*

303 Surface elemental composition of the thermally treated natural soils were determined with
304 X-ray photoelectron spectroscopy (XPS, analysis depth max. 10 nm). Recorded were
305 survey spectra with an Axis Ultra DLD device (Kratos Analytical, Manchester, UK), using
306 AlK α radiation (1486.7 eV) with 20 mA, 12 kV, and a pass energy of 160 eV. Spectra were
307 quantified with the software Vision 2 (Kratos Analytical, Manchester, UK), using the
308 implemented relative sensitivity factors.

309

310 *Contact angle (CA)*

311 CA was determined with the sessile drop method using a CCD equipped CA microscope
312 (OCA 15, Data Physics, Filderstadt, Germany). The material was fixed on a microscope
313 slide with double sided adhesive tape as a one-grain-layer and the placement of a drop (1
314 μL) of water recorded. Evaluated was the initial CA directly after placement of the drop and
315 ending of mechanical disturbances by drop shape analysis (ellipsoidal fit) and fit of
316 tangents on the left and the right side (Goebel et al., 2013). CA is given as the mean of six
317 drops ($n=12$).

318

319 **Results**

320

321 *DCDMS treatment effects*

322 The CA increased with increasing amount of the applied DCDMS. The texture of most
323 samples remained unaffected by the treatment of DCDMS (Table 1). There was one
324 exception, clay sample C1, which had been treated with the highest amount of DCDMS
325 showed an increase of the clay fraction in conjunction with an increase of the specific
326 surface area. DCDMS treatment increased the specific surface area for the fine sand
327 about 30% (SF), but increased the specific surface area for the silt sample by 30% (S) and
328 also for the clayey sample (C) by 20%. A comparison of the CA measurement before and
329 after the vapor bag experimental procedure of the isotope sampling confirmed the stability
330 of the coating for the field sand samples (values within the uncertainty of the
331 measurement, see Table 2). Additional increase of CA after the vapor bag experimental
332 procedure was observed for the silt samples. However, hydrophobicity created by DCDMS
333 treatment of the clay samples decreased after the entire experimental procedure (drying,
334 rewetting, isotope sampling and water potential measurement). The DCDMS treatment of
335 the clay samples resulted in initial CA of 51° and 105° directly after treatment. After drying
336 at 105°C , rewetting and isotope sampling, the initial CA of the clay sample treated with

337 400 μ l DCDMS/100g was reduced to from 51° to 18°, while the CA of the other clay sample
338 (1600 μ l DCDMS/100g) was reduced by 39° to 66°.

339

340 **Table 1**

341

342 *Thermal treatment effects*

343 The texture of the natural samples remained unaffected by heat treatment (Table 1).
344 Thermal treatment with 550°C decolorized the samples due to the removal of organic
345 compounds, increased the specific surface area and resulted in complete wettability,
346 i.e.CA=0°. Removal of the coating caused an increase in the content of the mineral-
347 derived cations (especially Si, Al, and Ca) and O and a decrease of C and N content within
348 XPS analysis depth (Table 3). The surface O/C ratio increased in accordance with an
349 increase in wettability, e.g. decrease of CA (Woche et al., 2017). While N was absent in
350 the interface after thermal treatment at 550°C, C content still was up to 20 at.-%, probably
351 due to adventitious carbon, i.e., carbon compounds adsorbed to the particle surfaces from
352 the surrounding air. Thermal treatment of the natural soil material at 105°C resulted in an
353 increase of C and a decrease of O content. Surface O/C ratio accordingly decreased after
354 105°C and CA increased. The specific surface area of the forest samples increased with
355 increasing temperature, while samples from the agricultural site did not show an effect by
356 thermal treatment on the specific surface area (Table 2). Effects temperature treatment on
357 the water retention characteristic and the equilibrium fractionation factor are depicted in
358 Figure 3.

359

360 **Table 2**

361 **Table 3**

362

363 *Water Retention Characteristics (WRC)*

364 The shape of the WRC of the DCDMS treated soil samples did not change in comparison
365 to the untreated control. Samples dried at 40°C and 105°C which were also changed in
366 CA, showed similar moisture release curves in the measured low-moisture range between
367 pF-value > 3 and pF-value < 6, like the silane-treated samples. The highest matric
368 potential values were observed above pF-value 5.5 (31.6 MPa) at 0.05 kg/kg water
369 content. In contrast, samples dried at 550°C reached a maximum soil tension of pF-value
370 4.5 (3.16 MPa). Most scatter of water content was observed between the different time
371 steps at or below wilting point, as indicated by the error bars (Figure 3). A change towards
372 higher soil tension over time was most pronounced for the samples dried at 40°C. Only
373 small variations in water content were observed for the samples dried at 105°C and 550°C.

374 **Figure 3**

375 *Isotope Retention Characteristic (IRC)*

376 The isotope retention characteristic (IRC) can be considered as an analogue to the water
377 retention characteristic. Instead of illustrating the relationship between matric potential and
378 water content, the IRC expresses the relationship between the matric potential ψ and the
379 equilibrium fractionation factor between bound water and water vapor (α_{x-y}). The isotope
380 retention characteristic is presented here for soil samples with different grain sizes and
381 different interfacial properties.

382 IRC's of the natural soil samples showed an increase of slope with increasing temperature
383 from 40° to 105°, while the 550° treated samples were similar to the 40° samples (Figure
384 3). Samples dried at 105°C plotted along the same regression line as found by Gaj and
385 McDonnell, (accepted), considering all values below pF-value 5. Values above pF-value 5
386 showed a decrease of α_{x-y} only for the samples dried at 105°C. The equilibrium
387 fractionation factor of samples dried at 40°C, steadily increased until pF-value 6. A less
388 distinct IRC was observed for the samples dried at 550°C. The error bars in Figure 3 for

389 the agricultural and the forest samples indicate the standard deviation of the equilibrium
390 fractionation factor α_{x-y} from the sampling after 1h, 24h, and 72h. A mean over the
391 standard deviation for all water contents for $\alpha^{18}\text{O}$ -values was $0.46 \cdot 10^{-4}$ for the sample
392 forest_40, $0.65 \cdot 10^{-4}$ for forest_105, and $0.75 \cdot 10^{-4}$ for forest_550. These values were
393 higher for the acre samples with $0.8 \cdot 10^{-4}$, $1.04 \cdot 10^{-4}$, and $1.4 \cdot 10^{-4}$ for acre_40, acre_105
394 and acre_550. Therefore, the most consistent fractionation factors with respect to small
395 standard deviation over time were observed for the samples dried at 105°C indicating
396 more stable and homogenous surface properties. The same standard deviation was
397 calculated for $\alpha^2\text{H}$ -values was $4.5 \cdot 10^{-4}$ for the sample forest_40, $4.8 \cdot 10^{-4}$ for forest_105,
398 and $5 \cdot 10^{-4}$ for forest_550. These values were higher for the acre samples with $4.3 \cdot 10^{-4}$,
399 $4.3 \cdot 10^{-4}$, and $4.8 \cdot 10^{-4}$ for acre_40, acre_105 and acre_550.

400 Dual isotope plots of the temperature treated soil samples are depicted in Figure 4.
401 Commonly a LEL derived from soil water isotope signatures relates two vertical distributed
402 variables to each other. The LEL shown here are a result of matric potential effects on the
403 equilibrium fractionation between the bound water and the water vapor. No actual
404 evaporation occurred during the experiment. The slopes of the evaporation lines of the
405 DCDMS – treated silt samples varied between 1 and 6.4 (Table 1); smaller slopes were
406 observed for the clay samples. Dual isotope plots of the natural soil samples grouped
407 according to the applied drying temperature. The slope of the LEL's of all-natural soil
408 samples changed slightly over the course of 3 days (expressed by the error bars).
409 Greatest slopes (6.6 – 15.9) were observed for the samples dried at 40°C . The δ -values
410 plot parallel to the GMWL. Generally, increasing CA can be attributed to higher slopes of
411 the evaporation lines (Figure 4 and Figure 5) until a $\text{CA}=90^\circ$. The slope of the evaporation
412 line decreases from 90° to higher CA's. The samples treated with 550°C do not fit into the
413 general picture. Neither the relationship between the contact angle and the O/C ratio, nor

414 the relationship between the slope of the evaporation line and the contact angle does align
415 to the other samples.

416 **Figure 4**

417

418 **Discussion**

419 *Matric potential, solid interfacial chemistry and wettability*

420 A shift in the WRC for water repellent soil samples towards lower matric potentials – as
421 shown by Lamparter et al., (2014) and Reszkowska et al., (2014) – was not observed in
422 this study for the analyzed soil samples and at the applied water content. Instead, our
423 observations are in agreement with a previous study that showed no or minor effects of the
424 wettability to the WRC at or around wilting point for hydrophobic and hydrophilic soil
425 samples with similar texture (Liu et al., 2012).

426

427 *IRC and wettability*

428 The physical properties controlling the storage and release of water are strongly related to
429 the surface chemical composition and the binding state of the water molecule layers
430 adsorbed to the particle surfaces. A change of the physicochemical structure of organic
431 matter has consequences for the mobility and adsorption of water (Diehl et al., 2014).
432 Sorption of non-polar organic compounds as well as heat treatment has a strong effect on
433 particle wettability (Decker and Ritsema, (1994); Reszkowska et al., 2014; Diehl et al.,
434 2014; Woche et al., 2017). This has corresponding effects on the spatial distribution of the
435 water content, on the binding state of thin water films on particles surfaces (Churaev,
436 2000) as well as on the shape and the radius of single water menisci (Muehl et al., 2012).
437 Consequently, this affects the energetic interfacial equilibrium state of the water vapor
438 pressure in a solid-water-vapor system and changes the equilibrium fractionation factor for
439 $^{18}\text{O}/^{16}\text{O}$ and $^2\text{H}/^1\text{H}$. However, as could be shown here the grain size distribution has the

440 major control to the isotopic equilibrium fractionation factor if non-polar organic compounds
441 are camouflages by surface hydroxyl groups of silane.

442

443 *IRC and surface chemistry*

444 In contrast, if the wettability is associated with the ratio of C/O the slope of the evaporation
445 line changes correspondingly. Therefore, our data provides evidence that the chemical
446 composition as expressed by the wettability of the particle surfaces affects the equilibrium
447 fractionation factor, i.e. the sessile drop contact angle might control the slope of the
448 evaporation lines without DCDMS (Figure 5). However, more data is needed to confirm
449 this relationship for both DCDMS and natural soil samples

450

451 *Secondary findings and future work*

452 The applicability of vapor bag equilibration method has been constrained by a lower limit of
453 3g of water within the bag (Wassenaar et al., 2008) due to water loss into the headspace
454 that enriches the original isotope signature of the sample. The data presented here have
455 already conclusively shown that not the water content by itself is the limiting factor to get
456 an unaffected isotopic signature with this method. It is merely the combination of soil
457 tension, the surface chemical composition and the wettability that controls the equilibrium
458 fractionation between tightly bound or immobile water and water vapor within the pore
459 space. Therefore, the isotopic signature of tightly bound water can be determined with the
460 vapor bag equilibration method if the IRC is known. This approach extends the applicability
461 of direct water vapor equilibration methods and consequently the use of in-situ
462 measurements.

463 As could be shown here, the drying of soil samples affects the surface properties and
464 changes the equilibrium fractionation factor. It is critical to develop a method for the
465 determination of the isotope retention characteristic of natural soil samples which does not

466 affect the surface properties. If other soil water extraction methods are affected by the
467 surface elemental conditions is not known.

468 **Figure 5**

469 **Conclusion**

470 We provide evidence that wettability, grain size distribution and the surface elemental
471 composition of solids affect the equilibrium fractionation factor in different ways. The
472 primary control on the equilibrium fractionation factor of soil water is the grain size
473 distribution. Secondly, the wettability, (as expressed by the contact angle) of surfaces has
474 an insignificant effect on the equilibrium conditions if the surface elemental composition is
475 camouflaged by DCDMS. However, the wettability controls the slope of the evaporation
476 line if water and water vapor can interact with the surface elemental composition of the soil
477 grain surface. This has been shown by soil samples that were treated with different
478 temperatures.

479 Therefore, the degree of transport, mixing and fractionation of water stable isotopes within
480 the unsaturated zone under drought is controlled by the composition of the biogeochemical
481 interface, soil tension and wettability. Further, the presented data has some important
482 implications from a methodical perspective. Sample preparation using oven dried samples
483 should consider that surface properties change and that this might affect the isotopic
484 signature of the bound water. Especially the use of stable isotope signatures of soil water
485 and water vapor at the dry end of the water retention curve (around wilting point) is largely
486 unexplored, but nevertheless important, since these dry conditions occur preferentially at
487 the shallow soil depths, where evaporation into the atmosphere occurs. These soil layers
488 are also enriched with organic matter changing wettability and solid particle interfacial
489 chemistry. Studies using soil water stable isotopes should consider corresponding
490 fractionation effects for better understanding and quantification of using stable water
491 isotopes for environmental studies. Neglecting these effects can bias application of direct

492 equilibration methods and calculations using models that assume equilibrium conditions
493 during soil water evaporation.
494

495 **References**

496

497 Bachmann, J., van der Ploeg, R. R. 2002. A review on recent developments in soil water
498 retention theory: interfacial tension and temperature effects, *J. Plant Nutr.* 165:468.

499

500 Bachmann, J., Deurer, M., Arye, G. 2007. Modeling water movement in heterogeneous
501 water-repellent soil: 1. Development of a contact angle–dependent water-retention model.
502 *Vadose Zone J.* 6: 436-445.

503

504 Bauters, T. W. J., Steenhuis, T. S., DiCarlo, D. A., Nieber, J. L., Dekker, L. W., Ritsema, C.
505 J., Parlange j.Y., Haverkamp, R. 2000. Physics of water repellent soils. *J. Hydrol.* 231:233-
506 243.

507

508 Barnes, C. J., Allison, G. B. 1983. The distribution of deuterium and ¹⁸O in dry soils: 1.
509 Theory, *J. Hydrol.* 60:141–156.

510

511 Barnes C.J., Allison G.B. 1984. The distribution of deuterium and ¹⁸O in dry soils: 3.
512 Theory for Non-isothermal Water movement, *J. Hydrol.* 74:119–135.

513

514 Barnes, C. J., Allison, G. B. 1988. Tracing of Water Movement in the unsaturated zone
515 using stable isotopes of hydrogen and oxygen, *J. Hydrol.* 100:143–176.

516

517 Bisdom, E. B. A., Dekker, L. W., Schoute, J. T. 1993. Water repellency of sieve fractions
518 from sandy soils and relationships with organic material and soil structure. *Geoderma*,
519 56:105-118.

520

521 Braud, I., Bariac, T., Biron, P., Vauclin, M. 2009a. Isotopic composition of bare soil
522 evaporated water vapor. Part II: Modeling of RUBIC IV experimental results. *J. Hydrol.*
523 369:17-29. doi:10.1016/j.jhydrol.2009.01.038

524

525 Braud, I., Biron, P., Bariac, T., Richard, P., Canale, L., Gaudet, J. P., Vauclin, M. 2009b.
526 Isotopic composition of bare soil evaporated water vapor. Part I: RUBIC IV experimental
527 setup and results. *J. Hydrol.* 369:1–16. doi:10.1016/j.jhydrol.2009.01.034

528

529 Brooks, R., Corey, T. 1964. Hydraulic Properties of Porous Media. *Hydrology Papers*,
530 Colorado State University.

531

532 Bowen G. 2015. Hydrology-The diversified economics of soil water, *Nature*. 43–45.

533

534 Churaev, N.V. 2000. Liquid and vapour flows in porous bodies: Surface phenomena.
535 Topics in chemical engineering Vol. 13, CRC Press.

536

537 Craig, H., Gordon, L.I., 1965. Deuterium and oxygen 18 variations in the ocean and the
538 marine atmosphere. *Stable Isotopes in Oceanographic Studies and Paleotemperatures*,
539 9–130, Pisa, Italy, Laboratorio di Geologia Nucleate.

540

541 Clark, I. D. Fritz, P. 1997. Environmental isotopes in hydrogeology, *CRC Press/Lewis*
542 *Publishers. Boca Raton. FL.* 328.

543

544 Coplen, T. B. 2011. Guidelines and recommended terms for expression of stable-isotope-
545 ratio and gas-ratio measurement results. *RCM*, 25(17), 2538-2560.

546

547 Dawson, T.E., Mambelli, S., Plamboeck A.H., Templer, P.H. and Tu, K.P. 2002. Stable
548 isotopes in plant ecology. *Annu. Rev. Ecol. Syst.* 33.

549

550 Dekker, L. W., Ritsema, C. J. 1994. How water moves in a water repellent sandy soil: 1.
551 Potential and actual water repellency, *Water Resour. Res.* 30:9, 2507–2517,
552 doi:10.1029/94WR00749.

553

554 Dongmann, G., Nürnberg, H. W., Förstel, H., & Wagener, K. 1974. On the enrichment of
555 H₂¹⁸O in the leaves of transpiring plants. *Rad and Environm Biophys.* 11:41-52.

556

557 Dubbert, M., Cuntz, M. M., Piady, A., Maguas, Werner, C. 2013. Partitioning
558 evapotranspiration - Testing the Craig and Gordon model with field measurements of
559 oxygen isotope ratios of evaporative fluxes, *J. Hydrol.* 496:142–153.
560 DOI:10.1016/j.jhydrol.2013.05.033

561

562 Diehl, D., Schneckenburger, T., Krüger, J., Goebel, M.-O. Woche, S.K., Schwarz, J. 2014.
563 Effect of multivalent cations, temperature and aging on soil organic matter interfacial
564 properties. *Environ. Chem.* 11:709. DOI: 10.1071/EN14008

565

566 de Jonge, L.W., Moldrup, P., and Jacobson, O.H. 2007 Soil-water content dependency of
567 water repellency in soils: Effect of crop type, soil management and physical-chemical
568 parameters. *Soil Science*, 172: 577-588.

569

570 Evaristo, J., Jasechko, S., McDonnell, J. J. 2015. Global separation of plant transpiration
571 from groundwater and streamflow. *Nature.* 525:91–94. DOI: 10.1038/nature14983

572

573 Gat, J. R., Bowser, C. J. and Kendall, C. 1994. The contribution of evaporation from the
574 Great Lakes to the continental atmosphere: estimate based on stable isotope data,
575 *Geophysical Research Letters*, 21, 557-560 452.

576

577 Garvelmann, J., Külls, C., Weiler, M. 2012. A porewater-based stable isotope approach for
578 the investigation of subsurface hydrological processes. *Hydrol. Earth Syst. Sci.* 16:631–
579 640. DOI: 10.5194/hess-16-631-2012

580 Gaj, M., Beyer, M., Koeniger, P., Wanke, H., Hamutoko, J., Himmelsbach, T. 2016. In situ
581 unsaturated zone water stable isotope (^2H and ^{18}O) measurements in semi-arid
582 environments: a soil water balance, *Hydrol. Earth Syst. Sci.*, 20:715–731.
583 doi:10.5194/hess-20-715-2016, 2016.

584

585 Gaj, M.; Kaufhold, S., Koeniger, P., Beyer, M., Weiler, M., Himmelsbach, T. 2017a. Mineral
586 mediated isotope fractionation of soil water. *Rapid Comm in Mass.* 31:269–280. DOI:
587 10.1002/rcm.7787.

588

589 Gaj, M.; Kaufhold, S.; McDonnell, J. J. 2017b. Potential limitation of cryogenic vacuum
590 extractions and spiked experiments. *Rapid Comm in Mass.* 31:821–823. DOI:
591 10.1002/rcm.7850.

592

593 Gaj, M. McDonnell, J.J. (under review): Soil tension controls the equilibrium fractionation
594 factor for soil water evaporation.

595

596 Gonfiantini, R. 1986. Environmental Isotopes in Lake Studies, 113–168. DOI:
597 10.1016/B978-0-444-42225-5.50008-5.

598

599 Goebel, M.-O., Woche, S. K., Abraham, P. M., Schaumann, G. E. & Bachmann, J. 2013.
600 Water repellency enhances the deposition of negatively charged hydrophilic colloids in a
601 water-saturated sand matrix. *Colloid Surf. A* 431, 150–160.

602

603 Gubiani, P. I., Reichert, J. M., Campbell, C., Reinert, D. J., Gelain, N. S. 2013. Assessing
604 Errors and Accuracy in Dew-Point Potentiometer and Pressure Plate Extractor
605 Measurements. *Soil Science Society of America Journal*. 77:19-24.

606

607 Good, S.P., Noone, D., Bowen, G. 2015. Hydrologic connectivity constrains partitioning of
608 global terrestrial water fluxes. *Science*. 349:175–177. DOI: 10.1126/science.aaa5931

609

610 Hassan, M., Woche, S. K., Bachmann, J. 2014. How the root zone modifies soil wettability:
611 Model experiments with alfalfa and wheat. *Journal of Plant Nutrition and Soil Science*,
612 177:449-458.

613

614 Hendry, M. J., Schmeling, E., Wassenaar, L. I., Barbour, S. L., Pratt, D. 2015. Determining
615 the stable isotope composition of pore water from saturated and unsaturated zone core:
616 improvements to the direct vapour equilibration laser spectrometry method, *Hydrol. Earth*
617 *Syst. Sci.* 19:4427–4440. doi:10.5194/hess-19-4427-2015

618

619 Horita J., Rozanski K., Cohen S. 2008. Isotope effects in the evaporation of water: a status
620 report of the Craig-Gordon model, *Isotopes Environ. Health Studies*. 44
621 doi:10.1080/10256010801887174

622

623 Klaus, J., Chun, K. P., McGuire, K. J., McDonnell, J. J. 2015. Temporal dynamics of
624 catchment transit times from stable isotope data, *Water Resour. Res.* 51:4208–4223,
625 doi:10.1002/2014WR016247

626

627 Koeniger, P., Marshall, J. D., Link, T., Mulch, A. 2011. An inexpensive, fast, and reliable
628 method for vacuum extraction of soil and plant water for stable isotope analyses by mass
629 spectrometry. *Rapid Commun. Mass Spectrom.* 25:3041–3048, doi:10.1002/rcm.5198

630

631 Koeniger, P., Gaj, M., Beyer, M., Himmelsbach, T. 2016. Review on soil water isotope
632 based groundwater recharge estimations. *Hydrol. Process.* doi:10.1002/hyp.10775. 2016.

633

634 Lamparter, A., Bachmann, J., Woche, S.K., Goebel, M., 2014. Biogeochemical Interface
635 Formation: Wettability Affected by Organic Matter Sorption and Microbial Activity. *Vadose*
636 *Zone J.* 13. DOI: 10.2136/vzj2013.10.0175.

637

638 Lin, Y., Horita, J. 2016. An experimental study on isotope fractionation in a mesoporous
639 silica-water system with implications for vadose-zone hydrology, *Geochim et Cosmo Acta.*
640 184:257–271. DOI: 10.1016/j.gca.2016.04.029

641

642 Liu, H., Ju, Z., Bachmann, J., Horton, R., Ren, T., 2012. Moisture-Dependent Wettability of
643 Artificial Hydrophobic Soils and Its Relevance for Soil Water Desorption Curves. *Soil*
644 *Science Society of America J.* 76:342. DOI: 10.2136/sssaj2011.0081

645

646 Majoube, M. 1971. Fractionnement oxygene 18 entre la glace et la vapeur d'eau." *J. of*
647 *Chem Phys.* 68.

648

649 McGuire, K. J., McDonnell, J. J. 2006. A review and evaluation of catchment transit time
650 modeling. *J. Hydrol*, 330(3-4), 543-563.

651

652 McDonnell, J. J. 2014. The two water worlds hypothesis: ecohydrological separation of
653 water between streams and trees? *WIREs Water*. 1:323–329. doi:10.1002/wat2.1027

654

655 Muehl, G. J. H., Rühlmann, J., Goebel, M. O., Bachmann, J. 2012. Application of
656 confocal laser scanning microscopy (CLSM) to visualize the effect of porous media
657 wettability on unsaturated pore water configuration. *Journal of soils and sediments*. 12:75-
658 85.

659

660 Mueller, M.H., Alaoui, A., Kuells, C., Leistert, H., Meusburger, K., Stumpp, C. 2014.
661 Tracking water pathways in steep hillslopes by $\delta^{18}\text{O}$ depth profiles of soil water. *J. of*
662 *Hydrol*. 519:340–352. DOI: 10.1016/j.jhydrol.2014.07.031

663

664 Oerter, E., Finstad, K., Schaefer, J., Goldsmith, G. R., Dawson, T., Amundson, R. 2014.
665 Oxygen isotope fractionation effects in soil water via interaction with cations (Mg, Ca, K,
666 Na) adsorbed to phyllosilicate clay minerals, *J. Hydrol*. 515:1–9.
667 doi:10.1016/j.jhydrol.2014.04.029, 2014.

668

669 Oerter, E. J., Bowen, G. 2017. In situ monitoring of H and O stable isotopes in soil water
670 reveals ecohydrologic dynamics in managed soil systems. *Ecohydrol*. 10:1841.
671 DOI:10.1002/eco.1841.

672

673 Othmer H., Diekkrüger, B. Kutilek 1991: Bimodal porosity and unsaturated conductivity.
674 *Soil Sci*. 152.3: 139-150.

675

676 Oshun, J., Dietrich, W. E., Dawson, T.E., Fung, I. 2016. Dynamic, structured heterogeneity
677 of water isotopes inside hillslopes. *Water Resour. Res.* 52:164–189. DOI:
678 10.1002/2015WR017485.

679

680 Orłowski, N., Pratt, D.L., McDonnell, J.J. 2016. Intercomparison of soil pore water
681 extraction methods for stable isotope analysis. *Hydrol. Process.* 30:3434–3449.
682 DOI:10.1002/hyp.10870.

683

684 Pronk, G. J., Heister, K., Vogel, C., Babin, D., Bachmann, J., Ding, G. et al. 2017.
685 Interaction of minerals, organic matter, and microorganisms during biogeochemical
686 interface formation as shown by a series of artificial soil experiments. *Biol Fertil Soils.*
687 53:9–22. DOI: 10.1007/s00374-016-1161-1

688

689 Peters, A., Sascha C. I., Durner W. 2015. Revisiting the simplified evaporation method:
690 Identification of hydraulic functions considering vapor, film and corner flow." *J. Hydrol.*
691 527:531-542.

692

693 Ritsema, C. J., Dekker, L. W. 1994. How water moves in a water repellent sandy soil: 2.
694 Dynamics of fingered flow. *Water resources research*, 30(9), 2519-2531.

695

696 Reszkowska, A., Bachmann, J., Lamparter, A., Diamantopoulos, E., Durner, W. 2014. The
697 effect of temperature-induced soil water repellency on transient capillary pressure–water
698 content relations during capillary rise. *European journal of soil science*, 65:369-376.

699

- 700 Rothfuss, Y., Vereecken, H., Brüggemann, N. 2013. Monitoring water stable isotopic
701 composition in soils using gas-permeable tubing and infrared laser absorption
702 spectroscopy. *Water resources research*, 49:3747-3755.
- 703
- 704 Rothfuss, Y., Braud, I., Le Moine, N., Biron, P., Durand, J.-L., Vauclin, M., Bariac, T. 2012.
705 Factors controlling the isotopic partitioning between soil evaporation and plant
706 transpiration: Assessment using a multi-objective calibration of SiSPAT-Isotope under
707 controlled conditions, *J. Hydrol.* 442-443:75–88. doi:10.1016/j.jhydrol.2012.03.041
- 708
- 709 Rothfuss, Y., Merz, S., Vanderborght, J., Hermes, N., Weuthen, A., Pohlmeier, A.,
710 Vereecken, H., and Brüggemann, N. 2015. Long-term and high-frequency non-destructive
711 monitoring of water stable isotope profiles in an evaporating soil column, *Hydrol. Earth*
712 *Syst. Sci.* 19:4067–4080. doi:10.5194/hess-19-4067-2015.
- 713
- 714 Rothfuss, Y., & Javaux, M. (2017). Reviews and syntheses: Isotopic approaches to
715 quantify root water uptake: a review and comparison of methods. *Biogeosciences*, 14:8,
716 2199.
- 717
- 718 Soderberg, K., Good, S. P., Wang, L., Caylor, K. 2012. Stable isotopes of water vapor in
719 the vadose zone: A review of measurement and modeling techniques, *Vadose Zone J.* 11.
720 doi:10.2136/vzj2011.0165
- 721
- 722 Sprenger, M., Herbstritt, B., Weiler, M. 2015. Established methods and new opportunities
723 for pore water stable isotope analysis. *Hydrol. Process.* 29:5174–5192. DOI:
724 10.1002/hyp.10643
- 725

726 Sprenger, M., Leistert H., Gimbel K., Weiler M. 2016. Illuminating hydrological processes
727 at the soil-vegetation-atmosphere interface with water stable isotopes. *Review of*
728 *Geophysics*. 54:674–704, doi:10.1002/2015RG000515

729

730 Stumpp, C., Maloszewski, P. 2010. Quantification of preferential flow and flow
731 heterogeneities in an unsaturated soil planted with different crops using the environmental
732 isotope $\delta^{18}\text{O}$. *J. Hydrol.* 394:407–415. doi:10.1016/j.jhydrol.2010.09.014

733

734 Skrzypek, G., Mydłowski, A., Dogramaci, S., Hedley, P., Gibson, J. J., Grierson, P. F.
735 2015. Estimation of evaporative loss based on the stable isotope composition of water
736 using Hydrocalculator, *J. Hydrol.* 523:781–789. doi:10.1016/j.jhydrol.2015.02.010

737

738 Van Genuchten, M. T. 1980. A closed-form equation for predicting the hydraulic
739 conductivity of unsaturated soils. *Soil Sci Soc of America*. 44: 892-898.

740

741 Vereecken, H.; SchnepF-value, A.; Hopmans, J. W.; Javaux, M.; Or, D.; Roose, T. 2016.
742 Modeling Soil Processes: Review, Key Challenges, and New Perspectives. *Vadose Zone*
743 *J.* 15. DOI: 10.2136/vzj2015.09.0131.

744

745 Volkmann, T., Weiler, M. 2014. Continual in-situ monitoring of pore water stable isotopes,
746 *Hydrol. Earth Syst. Sci.* 18:1819–1833. doi:10.5194/hess-18-1819-2014

747

748 Wassenaar, L. I.; Hendry, M. J.; Chostner V.L.; Lis G.P. 2008. High resolution pore water
749 ^2H and ^{18}O measurements by $\text{H}_2\text{O}_{[\text{liquid}]}$ - $\text{H}_2\text{O}_{[\text{vapor}]}$ equilibration Laser Spectroscopy,
750 *Environ Sci. Tech.* 4:9262–9267

751

752 West, A. G., Patrickson, S. J., & Ehleringer, J. R. 2006. Water extraction times for plant
753 and soil materials used in stable isotope analysis. *Rapid Comm. in Mass*, 20(8), 1317-
754 1321.

755

756 Woche, S. K. Goebel, M.; Mikutta, R., Schurig, C., Kaestner, M., Guggenberger, G.,
757 Bachmann, J. 2017. Soil wettability can be explained by the chemical composition of
758 particle interfaces - An XPS study. *Scientific Reports*. 7:42877. DOI: 10.1038/srep42877

759

760 Young, T. 1804. Experimental demonstration of the general law of the interference of light.

761 *Philosophical Transactions of the Royal society of London*. 94:1.

762

763

764 **Figure 1:** The color coding represents different water types such as mobile, immobile and
 765 hygroscopic water. If soils are saturated, water is moved by gravitation (blue). Availability
 766 of water for plant-root water uptake has its optimum at or around field capacity (green).
 767 During evaporation, a liquid network connects the soil water with the atmosphere. The
 768 dominant control on vapor pressure within the pore system is the soil temperature and the
 769 pore size. These two variables also define the threshold at which pore condensation
 770 occurs. If water is slowly available, then plants have water stress (orange). This is when
 771 the water within the pore system only forms thin water films on the soil particle surface. In
 772 this situation the influence of adhesion between the soil particle and the water controls the
 773 vapor pressure in addition to temperature. Liquid water transport only occurs via film flow.
 774 Water vapor diffuses through the soil profile driven by a vapor pressure gradient.
 775

776 **Figure 2: left:** A water drop on a plane surface develops a particular contact angle β
 777 depending on the solid's surface properties. An increasing contact angle causes the
 778 surface to be hydrophobic. A hydrophilic soil ($CA=0^\circ$), given a particular pore size
 779 distribution and water content, shows a higher soil water tension (or lower matric potential)
 780 compared to the same soil with reduced wettability ($CA>0^\circ$). The cohesion between water
 781 molecules dominates under hydrophobic conditions, the vapor pressure in the pore system
 782 and the equilibrium fractionation factor α , both are controlled by the soil temperature. In
 783 contrast, a hydrophilic surface causes adhesion between the soil particle surface and the
 784 water to control the vapor pressure and the equilibrium fractionation factor α .

785 **right:** The unsaturated pore system consists of three phases, the soil particle (solid), the
 786 liquid water and the water vapor. Soil particles in a natural system have a coating of
 787 particular physio-biogeochemical composition.

788 Artificial hydrophilization was created by treatment with dichloromethylsilane (DCDMS).
 789 Contact with water (the atmospheric humidity is sufficient) causes hydrolysis of the
 790 chlorine atoms that are intermediary replaced by hydroxyl groups that form hydrogen
 791 bonds with surface hydroxyl (silanol) groups. The hydrolyzed chlorine atoms react with
 792 hydrogen atoms to HCl gas that will evaporate or be dissolved in soil water. Soil water
 793 within the air-dry samples may favor HCl formation, possibly causing a drop in pH of the
 794 soil solution. Subsequent condensation results in a covalently bonded dimethyl siloxane
 795 (DMS) coating of the treated samples with the two methyl groups pointing towards pore
 796 space thus rendering the surface hydrophobic (Goebel et al., 2013; Hassan et al., 2014).
 797 Addition of different amounts of DCDMS varied the degree of reduction in wettability
 798 (Bachmann and Mc Hale, 2009). Hydrolyzed DCDMS units not involved in reaction with
 799 the particle surfaces will polymerize to form polydimethylsiloxane (PDMS) that may locate
 800 as water repellent particular bodies between the grains and may additionally affect CA.
 801 Heat treatment with 40°C , 105°C and 550°C affects the coating of the soil particle and
 802 creates different surface properties which has a strong effect on the wettability (Decker
 803 and Ritsema 1994, Reszkowska et al., 2014; Diehl et al., 2014).
 804

805 **Figure 3:** Water retention characteristics (top row), the equilibrium fractionation factor for
 806 ^{18}O (middle row) and the equilibrium fractionation factor for ^2H (lower row) are shown.
 807 Samples from the acre (left) and the forest (right) were treated with 40, 105, and 550°C .
 808 The heat treatment with 550°C reduced the matric potential compared to the treatment
 809 with lower temperature. Samples from the acre have a lower matric potential below wilting
 810 point compared to the forest soil. The equilibration time appeared to have an only minor
 811 impact on the moisture release curve and is indicated by the error bars. The equilibrium
 812 fractionation factor for ^{18}O increases with increasing soil tension (middle row). The dotted
 813 lines show the calculated equilibrium fractionation factor using the Kelvin-equation with a
 814 contact angle of 0° (upper curve) and a contact angle of 88° (lower curve). All values plot
 815 within the calculated equilibrium fractionation factors using the Kelvin equation. A

816 regression line found by Gaj and McDonnell (2018) is also indicated (dashed grey). Heat
817 treatment of the acre samples with 105°C resulted in higher slopes of $\alpha^{18}\text{O}$. In contrast,
818 $\alpha^2\text{H}$ does not show a strong effect on the shape of the isotope retention curve.
819

Figure 4: The global meteoric water line (dashed black), the local evaporation lines (LEL), their slope, intercept and R^2 are indicated in corresponding color coding. The heat treatment altered the wettability of the samples collected the acre and the forest. This caused a change of slope in dual isotope space, while all samples have the same grain size. Samples dried at 40° plot parallel to the GMWL. Heat treatment with 105° resulted in slopes which are found in arid zones. Drying at 550°C resulted in a slope between the two 40°C and 105°C sample sets.

820
821
822
823
824
825
826
827
828

Figure 5: The relationship between surface O and C (left), the surface O/C ratio and the contact angle (center) and contact angle with the slope of the local evaporation line (LEL) (right) are shown. Samples coated with DCDMS showed an increasing slope of the LEL along with an increasing CA. The heat-treated soils show a decrease of the C/O ratio and an increase of the contact angle. The slope of EL increased with increasing contact angle until 90° and decreased above that threshold. A relationship between grain size distribution and the slope of the LEL could not be found.

829 **Table 1:** The names of the samples are according to the German DIN standards for soil texture classifications. Particle size analysis, total organic
 830 carbon (TOC), total inorganic carbon (TIC) and applied DCDMS amount and surface area determined by BET analysis are summarized here. One set of
 831 samples were artificially hydrophobized using DCDMS as indicated. Samples from an acre and the forest with similar grain size but differenced in
 832 wettability were treated with 40, 105, and 550°C to alter surface properties.

Name	<63	63 - 630	630 -2000	μL DCDMS/100g	TOC [%]	TIC [%]	Surface Area [m ² /g]	Slope of the EL	R ² /p-value
SS	0	2.5	97.1	-	0.21 ±0.01	0	0.15	3.03	0.97 / <0.0001
SS_5	-	0	-	5			0.11	3.07	0.71 / 0.0012
Ut2_5	0	11.8	88.2	5	0.01 ±0	0	0.08	3.78	0.52 / 0.0052
Ut2_20	0	11.1	88.9	20			0.27	5.47	0.9 / 0.0001
Ut3	11.7	88.3	0.0	-			1.09	1.3	0.01 / 0.7251
Ut3_20	13.3	86.7	0.0	20	0.05 ±0.01	1.16 ±0.02	0.99	3.03	0.68 / 0.023
Ut3_60	13.2	86.8	0.0	60			0.81	3.65	0.87 / <0.0001
Su1	4.88	17.4	77.7	400	0.56 ±0.2	0	26.89	1.19	0.71 / 0.034
St3	24.11	3.9	72.0	1600			33.02	1.3	0.98 / <0.0001
SS_acre 40	0	7.9	92.1	-	2.06 ±0.15	0.23 ±0.01	0.11	7.75	0.85 / 0.0001
SS_forest 40	0	7.9	92.0	-	2.97 ±0.24	0.01 ±0.01	0.20	9.29	0.84 / <0.0001
SS_acre 105	0	5.6	94.3	-	1.70 ±0.03	0.28 ±0.03	0.12	1.94	0.52 / <0.0002
SS_forest 105	0	6.6	93.4	-	2.77 ±0.44	0.02 ±0.01	0.02	2.46	0.22 / <0.0329
SS_acre 550	0	4.2	95.7	-	0.02 ±0.0	0.21 ±0.04	0.57	4.71	0.65 / <0.0001
SS_forest 550	0	3.5	96.5	-	0.01 ±0.0	0	0.40	4.13	0.5 / 0.0011

833
 834
 835
 836
 837
 838
 839
 840
 841
 842

843

844 **Table 2:** Initial contact angle (CA_{ini}) and contact angles after 5s (CA_{5s}) of the DCDMS-treated samples were determined before (pre) and after (post)

845 determination of the IRC: The volumes given refer to the applied amount of DCDMS.

	CA _{ini}	CA _{5s}		
	(°)			
SS				
Orig	48.6	8.5	18.7	16.8
5 μL_{pre}	83.6	5.5	56.0	5.9
5 $\mu\text{L}_{\text{post}}$	70.1	10.1	62.6	12.6
10 μL_{pre}	93.6	7.3	81.3	12.0
10 $\mu\text{L}_{\text{post}}$	85.6	10.0	66.4	9.3
Ut2				
orig _{pre}	49.0	4.1	37.6	8.5
orig _{post}	53.5	6.1	31.2	8.9
5 μL_{pre}	111.0	7.0	96.4	9.9
5 $\mu\text{L}_{\text{post}}$	108.2	4.3	91.0	10.7
20 μL_{pre}	97.9	4.6	89.9	4.2
20 $\mu\text{L}_{\text{post}}$	91.0	6.7	73.3	5.3
Ut3				
orig _{pre}	13.7	4.3	0.0	0.0
orig _{post}	36.8	6.9	1.0	0.0
20 μL_{pre}	49.2	7.6	3.0	4.9
20 $\mu\text{L}_{\text{post}}$	73.5	4.6	40.7	4.9
60 μL_{pre}	60.2	5.1	27.8	7.7
60 $\mu\text{L}_{\text{post}}$	87.0	3.3	63.6	6.6
Su1 /St3				
400 μL_{pre}	52.6	9.8	1.0	0.0
400 $\mu\text{L}_{\text{post}}$	18.3	9.7	1.0	0.0
1600 μL_{pre}	104.5	9.5	61.5	6.0
1600 $\mu\text{L}_{\text{post}}$	66.3	13.3	22.3	17.2

846

847

Table 3: Surface chemistry of thermally treated soil samples determined by XPS analysis as atomic percentage of elements found. Additionally, initial contact angle (CA_{ini}) and contact angles after 5s (CA_{5s}) were determined and did not change.

	Na	Fe	O	N	Ca	K	C	Cl	P	Si	Al	Mg	O/C	Si/C	CA _{ini}	CA _{5s}																
	(at.-%)														(-)		(°)															
SS_ACRE																																
40_PRE	0.00	0.00	0.22	0.03	39.35	0.68	2.30	0.08	1.07	0.08	0.05	0.06	47.76	0.83	0.05	0.17	0.12	6.23	0.57	2.62	0.32	0.17	0.18	0.82	0.03	0.13	0.01	78.50	8.41	37.65	14.5	
40_AFT	0.00	0.00	0.03	0.03	40.82	0.98	1.44	0.20	0.02	0.02	0.01	0.01	44.50	0.58	0.04	0.05	0.02	0.03	12.38	0.74	0.69	0.25	0.06	0.06	0.92	0.03	0.28	0.02	102.00	5.10	87.66	11.1
105_PRE	0.05	0.05	0.05	0.05	34.36	1.74	2.85	0.11	1.07	0.05	0.00	0.01	54.86	2.66	0.02	0.02	0.23	0.10	4.26	0.56	2.11	0.39	0.16	0.07	0.63	0.06	0.08	0.01	122.79	6.80	116.24	5.7
105_AFT	0.00	0.00	0.09	0.03	33.18	1.23	2.66	0.20	1.10	0.07	0.01	0.01	56.24	2.13	0.01	0.01	0.24	0.01	4.19	0.43	2.11	0.38	0.18	0.14	0.59	0.04	0.07	0.01	122.73	9.35	120.07	10.1
550_PRE	0.05	0.02	0.51	0.12	54.80	3.76	0.09	0.11	4.35	0.28	0.03	0.02	20.65	5.89	0.00	0.01	1.11	0.06	11.87	1.85	5.93	0.64	0.60	0.31	2.83	0.95	0.62	0.26	1.00	0.00	0.00	0.0
550_Aft	0.00	0.00	0.46	0.12	56.73	1.66	0.03	0.03	4.33	0.54	0.02	0.02	20.29	3.52	0.24	0.08	0.88	0.12	8.30	0.50	7.83	1.25	0.89	0.29	2.86	0.53	0.42	0.06	1.00	0.00	0.00	0.0
SS_FOREST																																
40_PRE	0.01	0.01	0.07	0.07	36.70	1.06	1.52	0.26	0.03	0.01	0.01	0.02	50.83	2.51	0.02	0.01	0.03	0.01	10.27	1.79	0.45	0.09	0.07	0.04	0.72	0.06	0.20	0.04	105.37	10.65	90.36	11.9
40_AFT	0.00	0.01	0.16	0.07	38.28	0.27	2.98	0.09	1.22	0.05	0.01	0.01	49.18	0.76	0.03	0.02	0.27	0.06	5.38	0.60	2.24	0.08	0.25	0.17	0.78	0.02	0.11	0.01	91.40	7.36	54.04	9.7
105_PRE	0.00	0.00	0.05	0.05	33.76	0.92	1.27	0.05	0.07	0.03	0.01	0.01	53.96	1.86	0.02	0.02	0.03	0.03	10.07	0.98	0.65	0.09	0.11	0.07	0.63	0.04	0.19	0.02	129.17	6.13	124.01	9.0
105_AFT	0.00	0.01	0.05	0.05	31.22	2.00	1.19	0.12	0.06	0.03	0.00	0.01	57.96	3.73	0.01	0.01	0.02	0.02	8.86	1.56	0.50	0.05	0.13	0.12	0.54	0.07	0.15	0.04	134.50	15.66	130.28	13.8
550_PRE	0.14	0.06	0.28	0.12	59.73	2.15	0.03	0.03	0.37	0.04	0.25	0.33	15.00	4.27	0.02	0.02	0.08	0.06	20.33	2.09	3.49	0.15	0.28	0.08	4.25	1.45	1.47	0.58	1.00	0.00	0.00	0.0
550_Aft	0.09	0.02	0.64	0.07	58.44	2.48	0.04	0.04	0.83	0.11	0.15	0.05	16.97	3.74	0.06	0.04	0.24	0.07	15.27	0.78	7.07	0.46	0.19	0.05	3.57	0.83	0.93	0.23	1.00	0.00	0.00	0.0

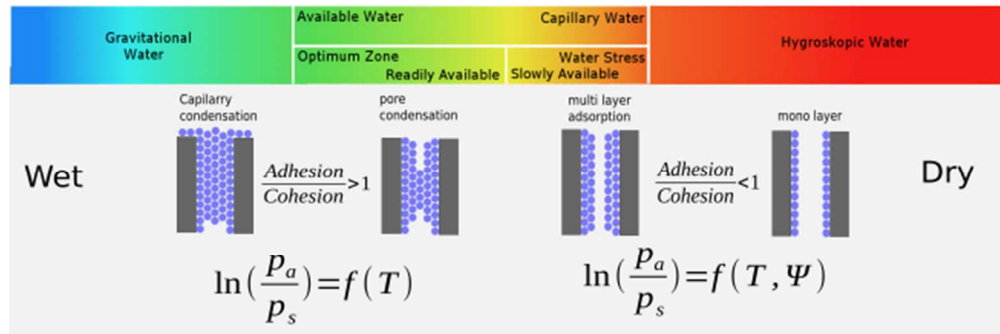


Figure 1: The color coding represents different water types such as mobile, immobile and hygroscopic water. If soils are saturated, water is moved by gravitation (blue). Availability of water for plant-root water uptake has its optimum at or around field capacity (green). During evaporation, a liquid network connects the soil water with the atmosphere. The dominant control on vapor pressure within the pore system is the soil temperature and the pore size. These two variables also define the threshold at which pore condensation occurs. If water is slowly available, then plants have water stress (orange). This is when the water within the pore system only forms thin water films on the soil particle surface. In this situation the influence of adhesion between the soil particle and the water controls the vapor pressure in addition to temperature. Liquid water transport only occurs via film flow. Water vapor diffuses through the soil profile driven by a vapor pressure gradient.

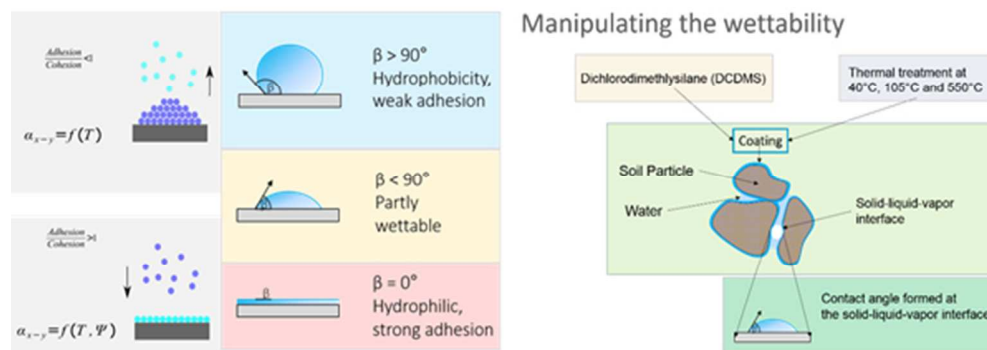


Figure 2: A water drop on a plane surface develops a particular contact angle β depending on the solid's surface properties. An increasing contact angle causes the surface to be hydrophobic. A hydrophilic soil ($CA=0^\circ$), given a particular pore size distribution and water content, shows a higher soil water tension (or lower matric potential) compared to the same soil with reduced wettability ($CA>0^\circ$). The cohesion between water molecules dominates under hydrophobic conditions, the vapor pressure in the pore system and the equilibrium fractionation factor α , both are controlled by the soil temperature. In contrast, a hydrophilic surface causes adhesion between the soil particle surface and the water to control the vapor pressure and the equilibrium fractionation factor α .

right: The unsaturated pore system consists of three phases, the soil particle (solid), the liquid water and the water vapor. Soil particles in a natural system have a coating of particular physio-biogeochemical composition.

Artificial hydrophilization was created by treatment with dichloromethylsilane (DCDMS). Contact with water (the atmospheric humidity is sufficient) causes hydrolysis of the chlorine atoms that are intermediary replaced by hydroxyl groups that form hydrogen bonds with surface hydroxyl (silanol) groups. The hydrolyzed chlorine atoms react with hydrogen atoms to HCl gas that will evaporate or be dissolved in soil water. Soil water within the air-dry samples may favor HCl formation, possibly causing a drop in pH of the soil solution. Subsequent condensation results in a covalently bonded dimethyl siloxane (DMS) coating of the treated samples with the two methyl groups pointing towards pore space thus rendering the surface hydrophobic (Goebel et al., 2013; Hassan et al., 2014). Addition of different amounts of DCDMS varied the degree of reduction in wettability (Bachmann and Mc Hale, 2009). Hydrolyzed DCDMS units not involved in reaction with the particle surfaces will polymerize to form polydimethylsiloxane (PDMS) that may locate as water repellent particular bodies between the grains and may additionally affect CA. Heat treatment with 40°C , 105°C and 550°C affects the coating of the soil particle and creates different surface properties which has a strong effect on the wettability (Decker and Ritsema 1994, Reszkowska et al., 2014; Diehl et al., 2014).

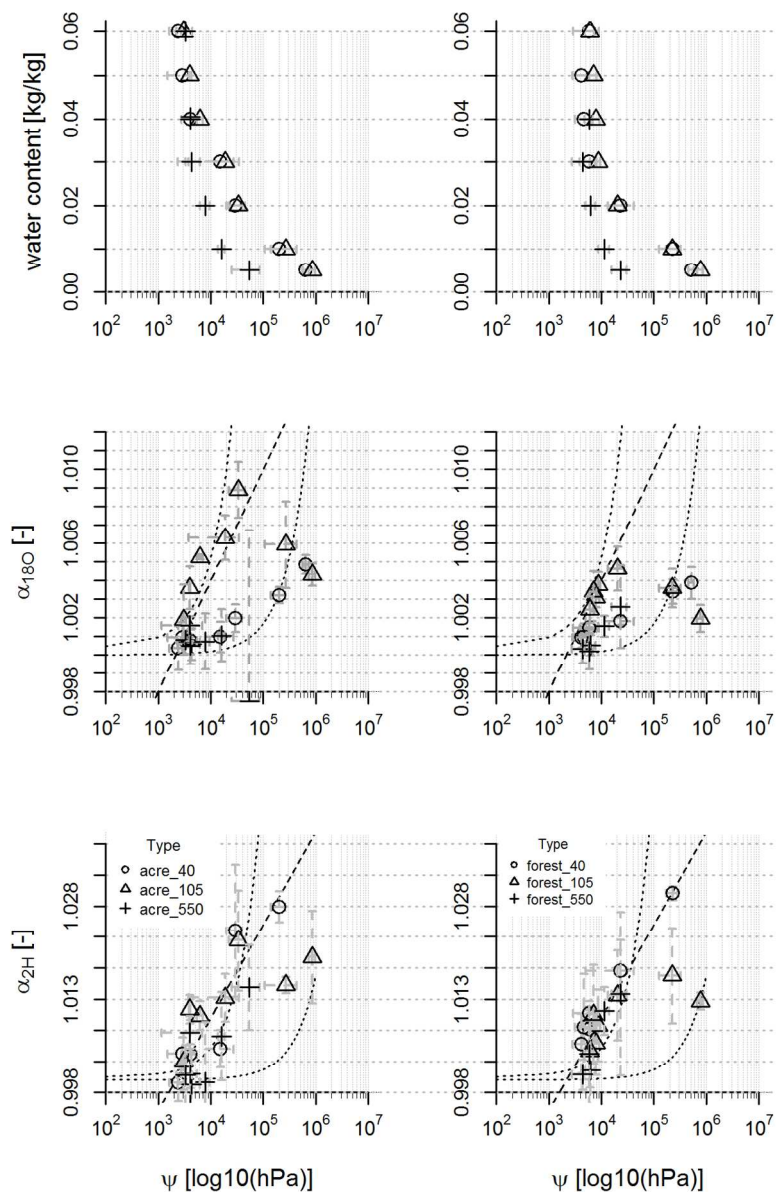


Figure 3: Water retention characteristics (top row), the equilibrium fractionation factor for 18O (middle row) and the equilibrium fractionation factor for 2H (lower row) are shown. Samples from the acre (left) and the forest (right) were treated with 40, 105, and 550°C. The heat treatment with 550°C reduced the matric potential compared to the treatment with lower temperature. Samples from the acre have a lower matric potential below wilting point compared to the forest soil. The equilibration time appeared to have an only minor impact on the moisture release curve and is indicated by the error bars. The equilibrium fractionation factor for 18O increases with increasing soil tension (middle row). The dotted lines show the calculated equilibrium fractionation factor using the Kelvin equation with a contact angle of 0° (upper curve) and a contact angle of 88° (lower curve). All values plot within the calculated equilibrium fractionation factors using the Kelvin equation. A regression line found by Gaj and McDonnell (2018) is also indicated (dashed grey). Heat treatment of the acre samples with 105°C resulted in higher slopes of α_{18O} . In contrast, α_{2H} does not show a strong effect on the shape of the isotope retention curve.

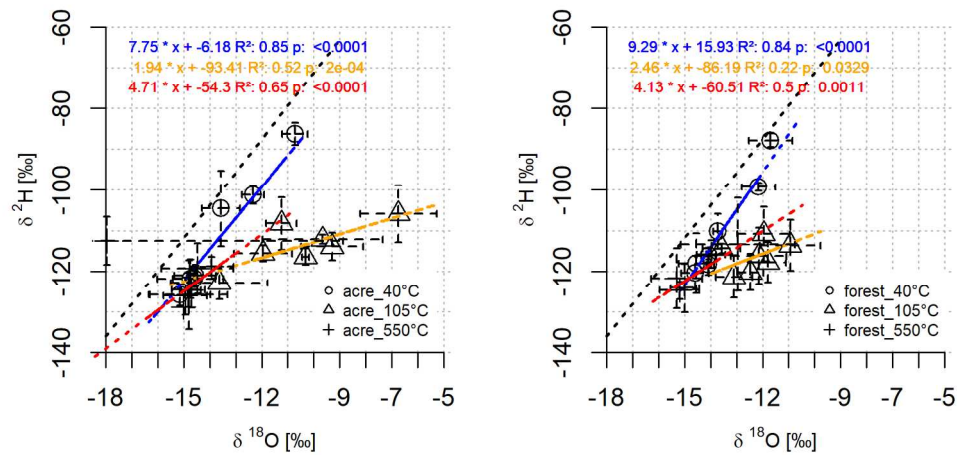


Figure 4: The global meteoric water line (dashed black), the local evaporation lines (LEL), their slope, intercept and R^2 are indicated in corresponding color coding. The heat treatment altered the wettability of the samples collected the acre and the forest. This caused a change of slope in dual isotope space, while all samples have the same grain size. Samples dried at 40° plot parallel to the GMWL. Heat treatment with 105° resulted in slopes which are found in arid zones. Drying at 550°C resulted in a slope between the two 40°C and 105°C sample sets.

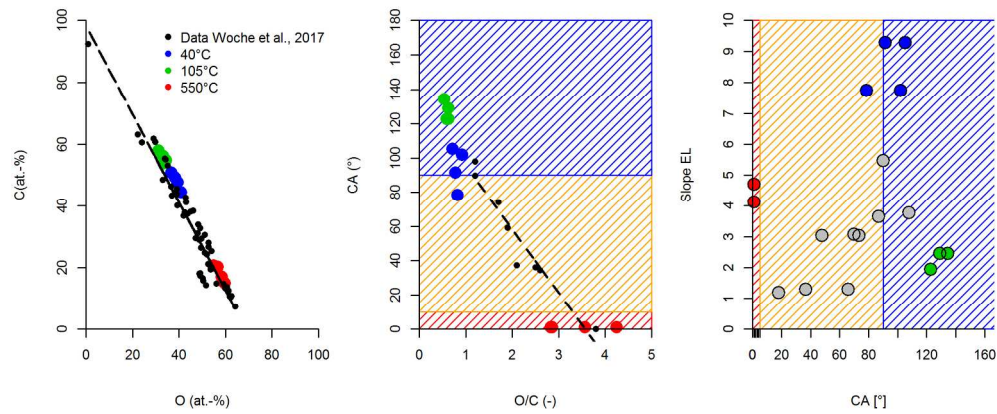


Figure 5: The relationship between surface O and C (left), the surface O/C ratio and the contact angle (center) and contact angle with the slope of the local evaporation line (LEL). (right) are shown. Samples coated with DCDMS showed an increasing slope of the LEL along with an increasing CA. The heat-treated soils show a decrease of the C/O ratio and an increase of the contact angle. The slope of LEL increased with increasing contact angle until 90° and decreased above that threshold. A relationship between grain size distribution and the slope of the LEL could not be found.